

Invited Paper

THz Photonics: The Synergy of Ultrafast Optics, Electronics, Micro-Microwaves and Quasi-Optics

Daniel R. Grischkowsky *

School of Electrical and Computer Engineering, Oklahoma State University, Stillwater, OK 74078, USA

*Email: daniel.grischkowsky@okstate.edu

(Received February 12, 2012)

Abstract: Ultrafast THz photonics has demonstrated the capability to create and to measure guided wave and freely propagating subps electrical pulses, which are much shorter than those produced and measured by any other method. THz photonics will be reviewed, starting with the use of photo-conductive switching on lithographically fabricated transmission lines on semiconductor chips. Lithographically fabricated, micron-sized antennas, when photo-conductively driven by subps laser pulses, radiate well into the THz regime. Freely propagating THz-TDS and Waveguide THz-TDS measurements will be presented. Future opportunities in fundamental research and practical applications, including THz communications, will be described.

Keywords: THz-TDS, Quasi-Optics, Photoconductive Switching, and THz Communications

doi: [10.11906/TST.048-066.2012.03.05](https://doi.org/10.11906/TST.048-066.2012.03.05)

1. Introduction

Optoelectronic techniques combining ultrafast laser pulses, photoconductive switching [1] and VLSI lithography have enabled the generation and measurement of subps electrical pulses propagating as a single-mode excitation on co-planar transmission lines [2]. These pulses can also be used to characterize the transmission line itself and attached electronic devices. Photoconductive switching has also enabled the development of a complete optoelectronic, quasi-optically coupled THz beam system with high signal to noise response out to 5 THz. These developments and their applications will now be described.

The subps electrical pulses shown in Fig. 1 were obtained by photoconductively shorting a charged 5- μm coplanar transmission line with 80 fs laser pulses [2]. The electrical pulses were measured by a fast photoconductive switch (gap), driven by a time delayed beam of the same 80 fs laser pulses, which connected the transmission line to an electrical sampling probe. This method of excitation is especially well matched to the propagating mode of the transmission line. After 8 mm of propagation on this line, the pulses broadened to 2.6 ps.

For the geometry of the experiment shown in Fig. 1, the 20-mm-long transmission line had a design impedance of 100 Ω and was made of two parallel 5 μm -wide aluminum lines separated from each other by 10 μm . The dc resistance of a single 5 μm line was 200 Ω . Because of the small dimensions, the geometrical dispersion of this line is much less than an equivalent micro-

strip line. The laser spot diameters were both $10\ \mu\text{m}$. It is important to note that the excitation beam can continuously move and that no special lithographic features are required for the pulse generation. Consequently, we have the equivalent of a “sliding contact” for the excitation beam. The transmission line together with its pads and sampling gaps was fabricated on an undoped commercial (Union Carbide UCC-O) silicon on sapphire (SOS) wafer. The transmission line pattern was defined by conventional photolithographic lift-off techniques. To ensure the required short carrier lifetime, the wafer with the Al transmission line pattern was implanted with two doses of O^+ ions, $1.0 \times 10^{15}/\text{cm}^2$ at $200\ \text{keV}$ and $1.0 \times 10^{15}/\text{cm}^2$ at $100\ \text{keV}$

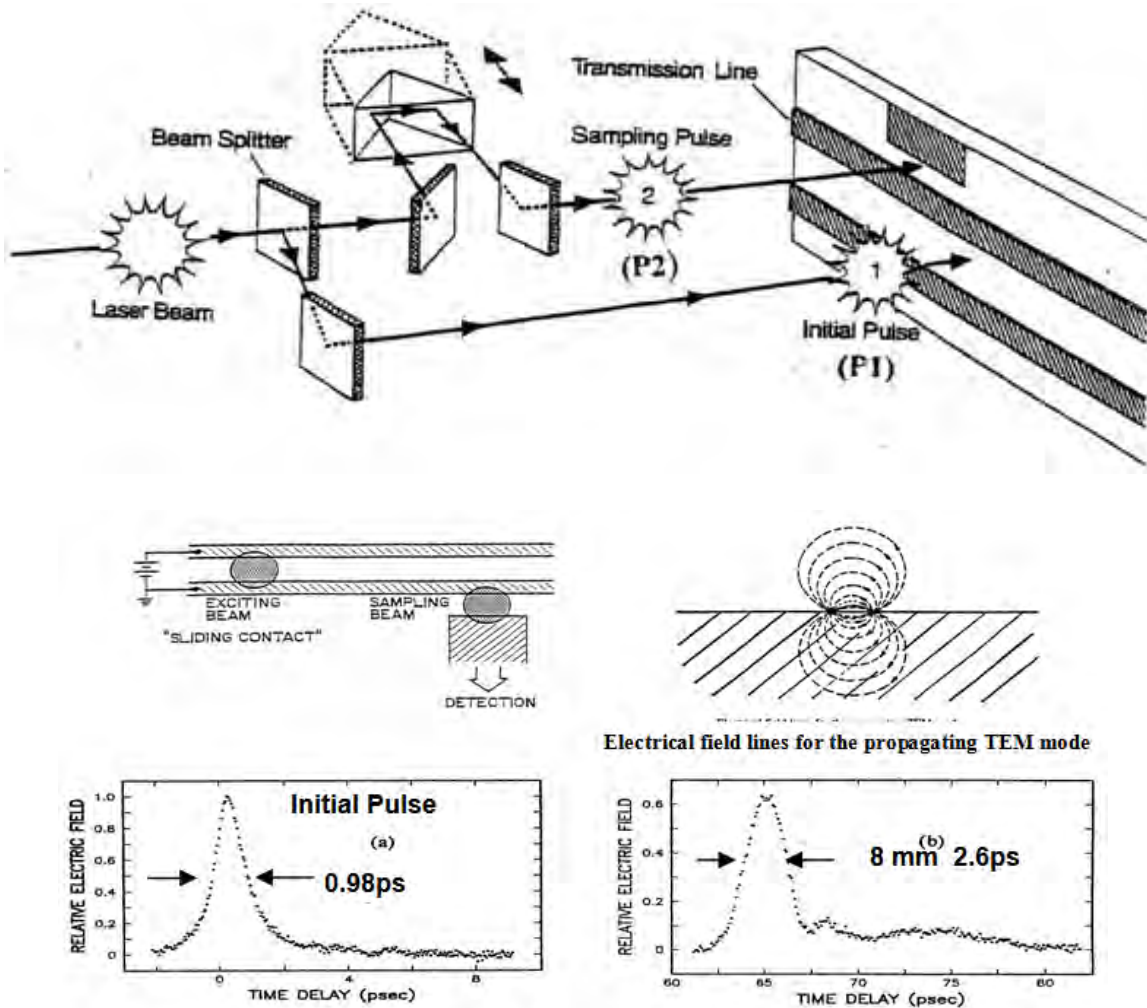


Fig. 1 The performance of THz photonics is demonstrated by the first observation of a subps electrical pulse on chip . The measurement of the $0.98\ \text{ps}$ FWHM pulswidth with a signal-to-noise ratio (S/N) of better than 1000 was more than 30 years ahead of what could be obtained from electronics alone. The schematic of the measurement is shown, as well as the broadening and attenuation effects on the pulse that had propagated $8\ \text{mm}$ down the transmission line.

Consideration of the sliding contact excitation site in Fig. 1 shows that, to first order, charge is simply transferred from one line to the other creating a symmetrical field distribution with respect

to the two lines. During the excitation process, a current flow is induced between the lines. Localized charge accumulations of opposite sign build up on the segments of the two metal lines under the laser excitation spot, creating a dipolar field distribution similar to that of the TEM mode shown in Fig. 1. This situation provides an excellent broad band coupling to the propagating TEM mode of the transmission line [3].

The severe broadening and loss suffered by the propagating electrical pulse after only 8 mm of propagation on the transmission line, as shown in Fig.1, could not be explained by the existing VLSI propagation codes for on-chip pulses. This loss was later explained by an electromagnetic shock wave from the propagating dipole on the transmission line [4]. The Cherenkov type shock wave occurred because the dipole was propagating faster than the speed of light in the dielectric substrate. A numerical analysis of this effect for our conditions gave a good agreement with the observations [4]. A schematic drawing of the Cherenkov shock wave is given below in Fig. 2.

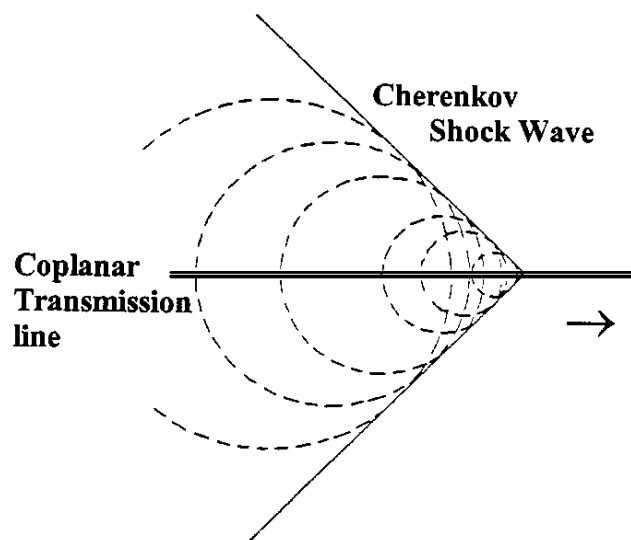


Fig. 2 the Cherenkov radiation cone in the dielectric substrate half space

2. Generation of THz radiation at the excitation point

The electrical and quasi-optical set-up shown in Fig. 3 generated and measured the strong freely propagating THz radiation pulse, which was generated together with the subps electrical pulse on the transmission line [5]. With the simple photo-conductive switch, THz wave detector was driven by a carefully focused and synchronized beam of ultrafast laser sampling pulses. Compared to the measured pulse on the transmission line, the measured THz radiation pulse was surprisingly strong and appeared with the expected derivative of the line-pulse shape. The measured pulse delay was in an accurate agreement with that determined by the THz index of refraction for the total path in the solid sapphire hemisphere.

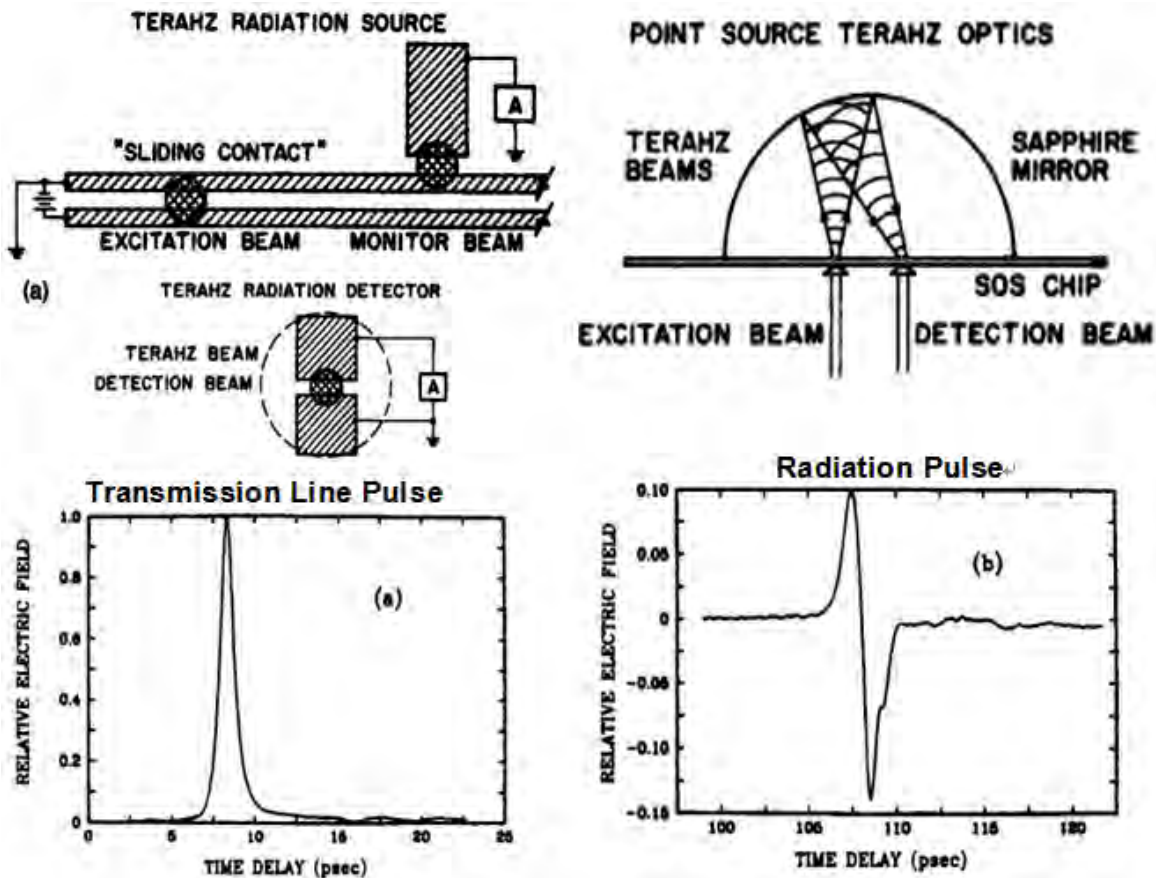


Fig. 3 Schematic diagram of the charged coplanar transmission line. The laser excitation spot defines the location of the transient electric dipole. The monitor beam measures the electrical pulse coupled to the line. Schematic diagram of the THz detector. The laser detection beam spot is shown centered on the gap in the focal spot (dashed circle) of the THz radiation. Schematic diagram of the the focusing optics consisting of a gold-coated, solid-hemispherical sapphire mirror with a diameter of 9.5 mm in contact with the backside (sapphire side) of the SOS chip. (a) Measured electrical pulse with 120 μm separation between the excitation and monitor beams. (b) Measured electrical pulse of the focused freely propagating THz pulse at the detector.

The two main features of our method are clearly evident by the measurement of Fig. 3b. Firstly, excellent time resolution is obtained as shown by the 1 ps duration from the maximum to the minimum. Secondly, the collection is exceptionally efficient. The measured radiation pulse has a very good signal-to-noise ratio and the peak to peak amplitude is approximately 25% of that of the pulse coupled to the lines. Considering that only the central 10 μm -diam of the total 100- μm -diam focal spot of the THz radiation is detected, the power in the radiated THz pulse appears to be approximately the same as that coupled onto the transmission lines. Our experimental results showed that, by using standard quasi-optical components and techniques combined with point sources of THz radiation, it would be possible to generate well collimated beams of freely propagating subps THz pulse for a multitude of applications.

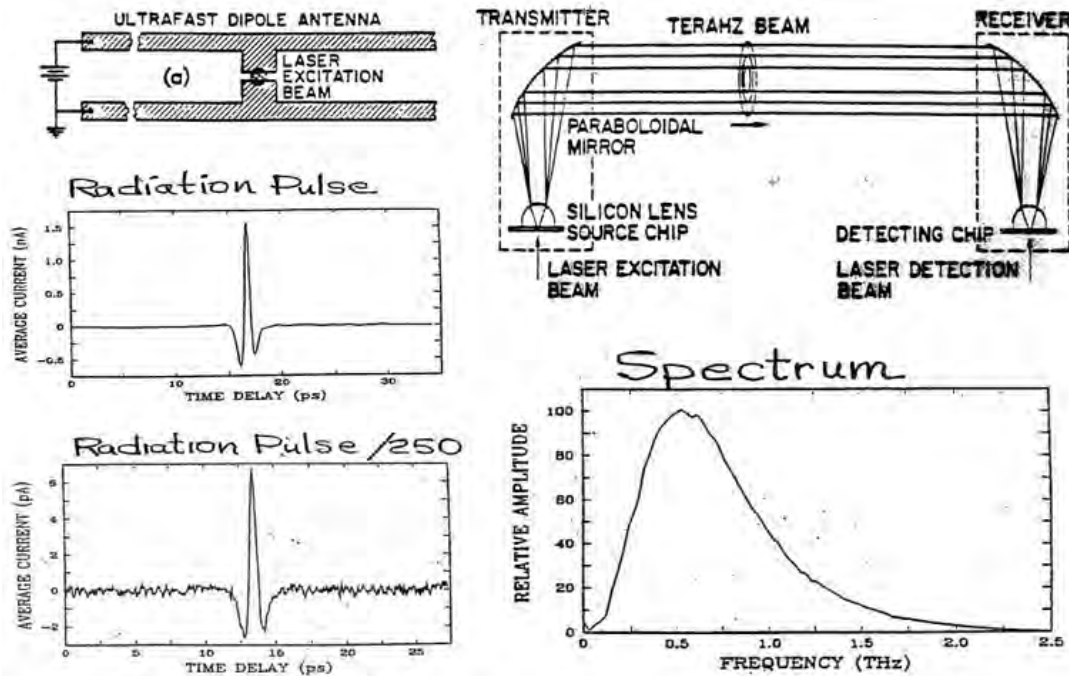


Fig. 4 The first complete THz Optoelectronic Beam System (1990). The ultrafast photo-conductive dipole antenna is shown together with the THz quasi-optical set-up of the complete THz transmitter and THz receiver used for THz time-domain spectroscopy (THz-TDS). Driven by excitation and sampling beams of ultrafast optical pulses, this system generates and measures sub-ps THz pulses with an amplitude S/N of 10,000, and is still being used today.

The developed optoelectronic THz setup used to generate and detect beams of short pulses of THz radiation is presented in Fig. 4 [7]. The transmitting and receiving antennas are identical, each consisting of the antenna imbedded in a coplanar transmission line. The antennas are fabricated on an ion-implanted silicon-on-sapphire (SOS) wafer. The $20\ \mu\text{m}$ -wide antenna structure is located in the middle of a 20-mm -long coplanar transmission line consisting of two parallel $10\ \mu\text{m}$ -wide, $1\ \mu\text{m}$ -thick, $5\ \Omega/\text{mm}$, aluminum lines separated from each other by $30\ \mu\text{m}$. In this initial demonstration, a colliding-pulse mode-locked (CPM) dye laser produced $623\ \text{nm}$, $70\ \text{fsec}$ pulses at a $100\ \text{MHz}$ repetition rate in a beam with $5\ \text{mW}$ average power. This beam was focused onto the $5\text{-}\mu\text{m}$ -wide photoconductive silicon gap between the two antenna arms. The $70\ \text{fsec}$ laser creation of photocarriers causes subps changes in the conductivity of the antenna gap. When a DC bias voltage of typically $10\ \text{V}$ is applied to the transmitting antenna, these changes in conductivity result in pulses of electrical current through the antenna, and subsequent bursts of electromagnetic radiation are produced. A large fraction of this radiation is emitted into the sapphire in a cone normal to the interface. This radiation is then collected and collimated by a dielectric lens attached to the backside (sapphire side) of the SOS Wafer [6-8]. Here, the dielectric lenses were made of high-resistivity ($10\ \text{k}\Omega\text{cm}$) Si, which has a measured absorption of less than $0.05\ \text{cm}^{-1}$ up to $3\ \text{THz}$ [8-9]. The center of the truncated $9.5\ \text{mm}$ diameter silicon sphere (lens) is $2.0\ \text{mm}$ above the ultrafast antenna located at the focus of the lens. After collimation by the silicon lens, the beam propagates and diffracts to a paraboloidal mirror, where the THz radiation is recollimated into a highly directional beam. The combination of the paraboloidal mirror and the silicon lens (THz optics) and the antenna chip comprise the transmitter, the source of a highly-directional freely-propagating beam of subps THz pulses. After a $50\ \text{cm}$ propagation

distance, this THz beam was detected by an identical combination, the THz receiver, where the paraboloidal mirror focuses the beam onto the silicon lens, which focuses it onto a SOS antenna chip, similar to the one used in the emission process. The electric field of the focused incoming THz radiation induces a transient bias voltage across the $5\ \mu\text{m}$ gap between the two arms of this receiving antenna, directly connected to a low-noise current amplifier. The amplitude and time dependence of this transient voltage is obtained by measuring the collected charge (average current) versus the time delay between the THz pulses and the delayed CPM laser pulses in the $5\ \text{mW}$ detection beam. These pulses synchronously gate the receiver, by driving the photoconductive switch defined by the $5\ \mu\text{m}$ antenna gap.

A typical time-resolved measurement is also shown in Fig. 4 [7]. The clean pulseshape is a result of the fast action of the photoconductive switch at the antenna gap, the broadband response of the ultrafast antennas, the broadband THz optical transfer function of the lenses and the paraboloidal mirrors, and the very low absorption and dispersion of the silicon lenses. The measured pulsewidth of $0.54\ \text{ps}$ (FWHM) is only an upper limit to the true pulsewidth, because no deconvolution has been applied to the measurement to take out the response time of the antenna gap.

The Fourier transform of the measured signal is shown to stretch from about 0.1 to $2.0\ \text{THz}$. This represents only a lower limit to the true extent of the emitted radiation as it contains the frequency response of the receiver. Another scan of the output pulse is shown for which the intensity of the pump laser beam was reduced from the $6\ \text{mW}$ normally used to only $15\ \mu\text{W}$. This 400-fold reduction in laser power led to a reduction in the transient photocurrent of 250 instead of the expected 400. The discrepancy indicates a slight nonlinearity due to the onset of saturation, related to the fact that the electrical pulses generated on the transmission line are quite strong (almost $1\ \text{V}$ in either direction). This 250-fold reduction in photocurrent led to a reduction in the power of the THz beam by the factor 1.6×10^{-5} . However, despite this enormous reduction in power, the peak amplitude S/N is still more than 30. If the power of the THz beam were even further reduced, the detection limit of the THz receiver would be reached a $1/10^{-16}\ \text{W}$. Because the generation and detection of the THz radiation is coherent, the THz receiver is intrinsically much more sensitive than the incoherent bolometer. Here, the receiver is approximately 1000 times more sensitive than a helium cooled bolometer [10].

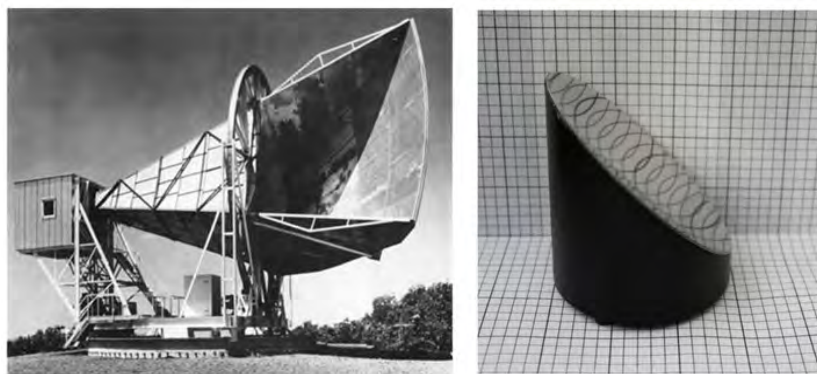


Fig. 5 The famous horn antenna at the Bell Telephone Laboratories, Holmdel, New Jersey, USA, which first observed the residual black-body radiation in the universe, is compared to the paraboloidal mirror used in the THz Optoelectronic Beam System.

The technical potential of THz quasi-optics is shown by the comparison of the relative size (small squares are 5 mm) and beam divergence of the paraboloidal mirrors used in the THz-TDS system to that of the precisely made microwave antenna shown in the photograph, which made the first observation of the black body radiation from the big bang creation of the universe [11]. This antenna is 50 ft (15.24m) long with a radiation aperture of 20x20 ft (6.1m); the operating frequency was 4.08 GHz with a wavelength of 7.35 cm. The radiation aperture is 83x83 wavelengths. In contrast, the paraboloidal mirrors have optical precision with a 76.2 mm diameter and a 125 mm focal lengths. The 1 THz wavelength is 0.300 mm. The corresponding aperture diameter is 254 wavelengths, thereby giving better performance together with a size reduction of 100.

3. THz Waveguides

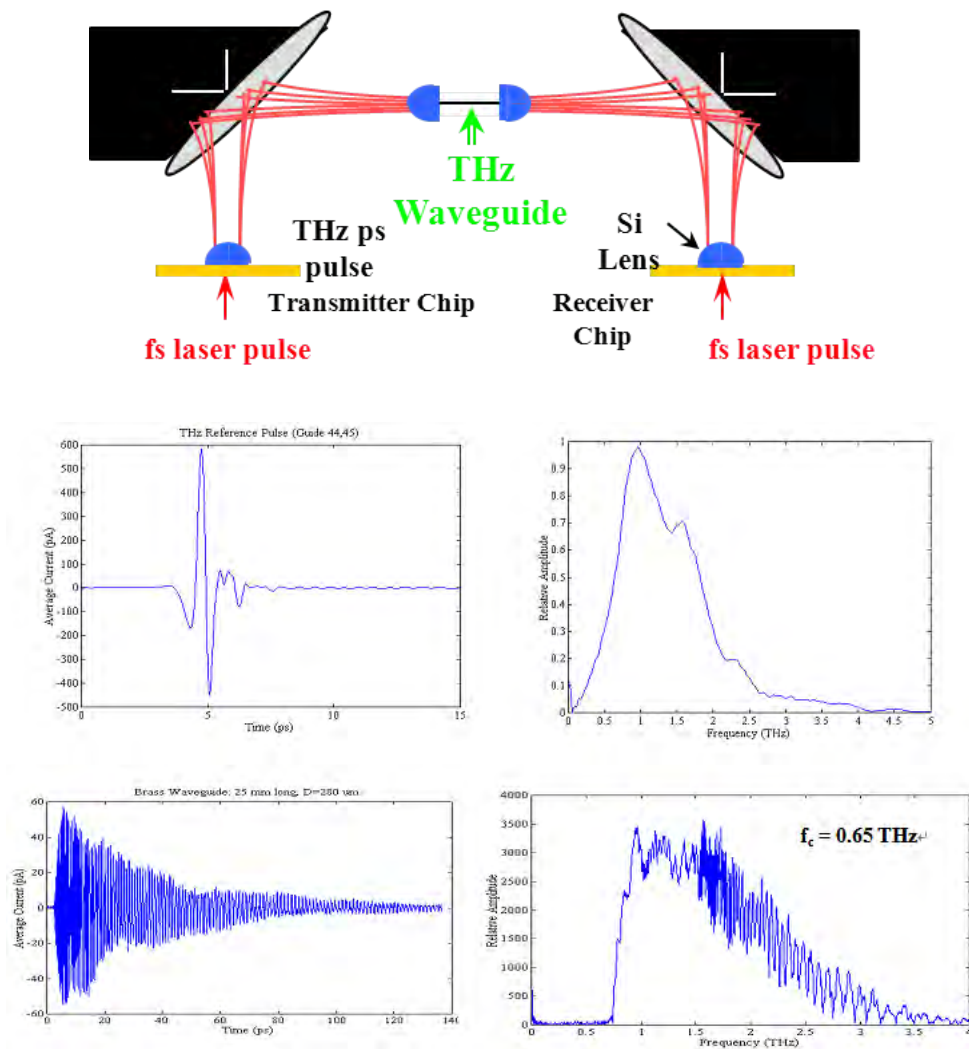


Fig. 6 Schematic and results of THz waveguide investigations. Quasi-optical coupling into the waveguides placed in the center of the THz-TDS system is surprisingly efficient. Metal tube waveguides with either circular or rectangular cross sections have very high group velocity dispersion near the cut-off wavelengths.

These experimental investigations showed that quasi-optical methods can be used to efficiently couple freely propagating, optoelectronically generated, subps pulses of THz radiation into submillimeter circular metal tubes (waveguides) and consequently, to measure the transmitted pulses from these waveguides [12-13]. Very dispersive low-loss propagation was observed over the frequency band from 0.65 to 3.5 THz, with frequency dependent group velocities v_g ranging from $c/4$ to c and phase velocities v_p from $4c$ to c , where $v_g v_p = c^2$, as expected from classical waveguide theory. Even though the input spectrum overlapped the cutoff frequencies of more than 25 waveguide modes, the linearly polarized incoming THz pulses significantly coupled only into five modes for the circular waveguides and four modes for the rectangular waveguides. Using classical waveguide theory, the coupling coefficients into the modes of the waveguides were calculated for the incoming focused THz beam. The propagation of the THz pulse through the waveguide was described as a linear superposition of the coupled propagating modes, each with a unique complex propagation vector. It was shown that this superposition of the propagating modes explained all of the observed features of the complicated THz output pulse.

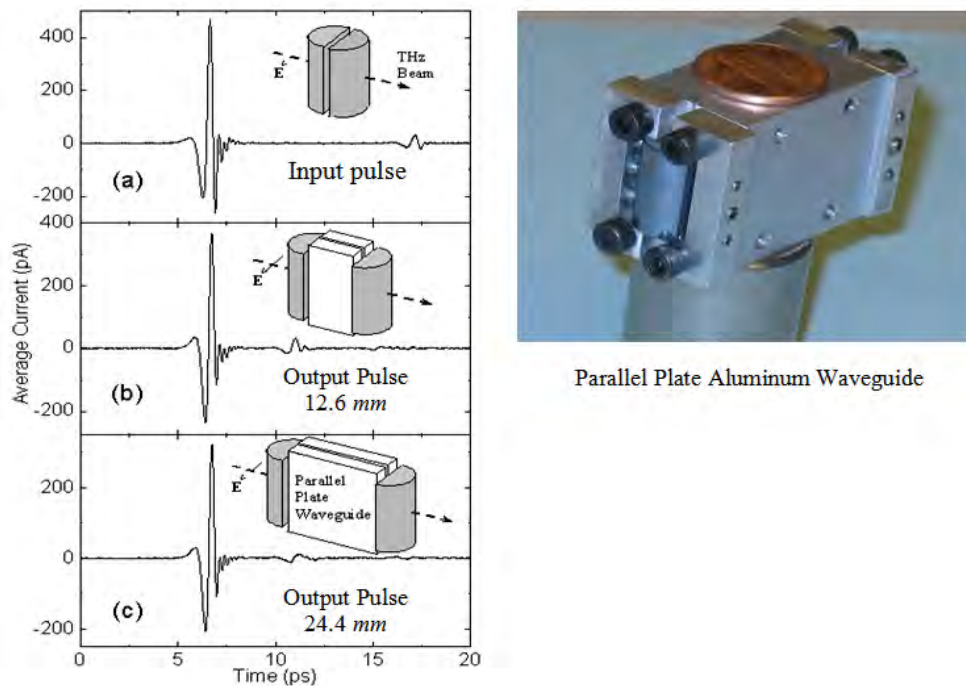


Fig. 7 TEM mode propagation through a parallel plate waveguide (PPWG) with a plate separation of $108 \mu\text{m}$. (a) Measured THz reference pulse with only the confocal cylindrical lens system in place. (b) Measured THz transmitted pulse through the 12.6 mm short PPWG. (c) Measured THz transmitted pulse through the 24.4 mm long PPWG.

In contrast to the circular and rectangular metal tube waveguides, excessive pulse broadening due to GVD will not occur for the TEM mode of a two-wire coplanar line, a twinline cable, a coaxial cable, or for a parallel plate waveguide (PPWG). Unfortunately, quasi-optic coupling techniques cannot couple to the complex field patterns of the TEM mode of twinline or coaxial cable. However, efficient coupling is possible for the simple field pattern of the TEM mode of

the PPWG. The first demonstrations of TEM propagation through the THz PPWG are shown in Fig. 7. The excellent propagation properties of the PPWG have made possible waveguide THz-TDS [14-15].

After the above demonstration, a physically flexible, 250 mm long THz PPWG was demonstrated, which showed minimal pulse distortion and loss [16]. The waveguide was constructed using two 100 μm thick copper strips 35 mm wide and 250 mm long. They were joined together lengthwise by double-sided adhesive tape 10 mm wide and 90 μm thick, which provided an air-space, having cross-sectional dimensions of 90 μm x 15 mm between the plates. TEM mode propagation was preserved as long as the axial changes in the waveguide (bends and twists) are spatially small compared to the propagating wavelengths [17]. Efficient quasi-optic coupling into these waveguides was demonstrated. The observed attenuation was mainly due to the finite conductivity of copper with some loss due to diffractive beam spreading in the unguided dimension. The observed pulse broadening was due to the frequency dependent loss since GVD was negligible.

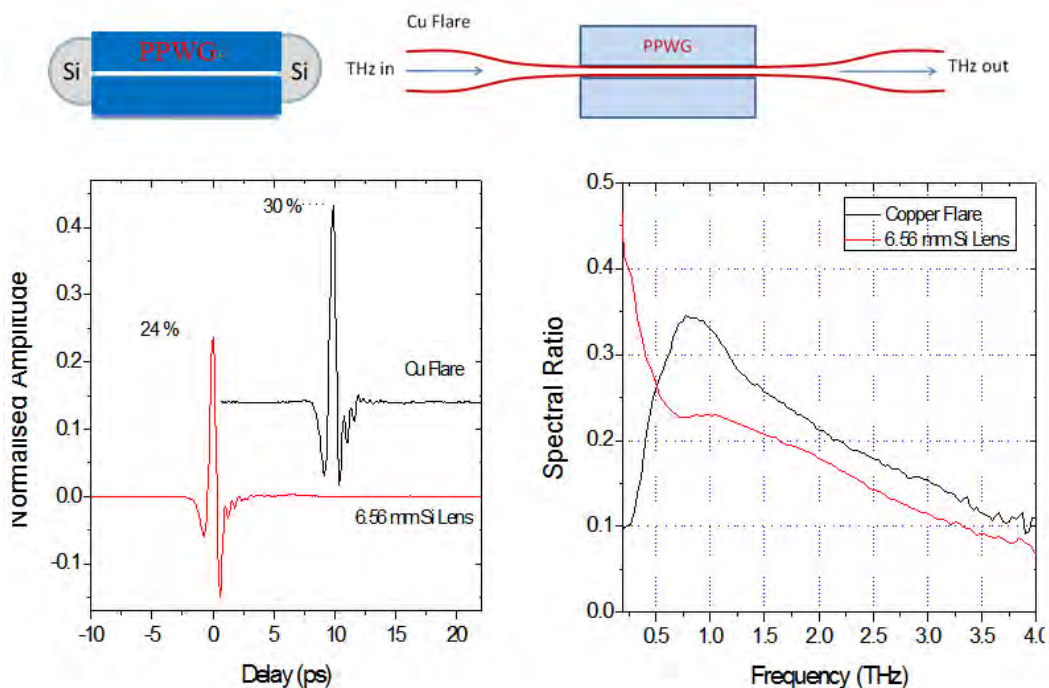


Fig. 8 The coupling efficiency of high-resistivity Si cylindrical lenses to a PPWG is compared to horn antennas.

As the THz frequency band is located between microwaves and the infrared, coupling schemes known in both domains can be used. The quasi-optical method using lenses is the infrared approach. Recently the well known microwave approach based on curved metal surfaces (horn antenna) was used to couple linearly polarized THz radiation into the parallel plate waveguide (PPWG) and to compare the performance to silicon lens coupled PPWGs [17]. In the quasi-optical approach, the metal surface would just reflect the THz waves. But, if the changes in the beam extent are introduced adiabatically [18], which denotes slowly with respect to the wavelength, the reflection losses can be minimized and propagation in the forward direction is maintained.

This type of coupling is nearly distortionless as seen in Fig. 8, where the transmitted pulses using flare coupling and using the quasi-optic coupling with Si cylindrical lenses are directly compared. As can be observed, with flare coupling the transmitted pulse is significantly larger. The associated amplitude spectra of these pulses are also compared, where above 0.5 THz the flare amplitude spectra is also significantly larger. The main reason for this difference is that the quasi-optic coupling suffers severe Fresnel reflection losses from the high THz index of refraction $n = 3.42$ of Si, causing the amplitude transmission to be reduced by the factor of 0.5.

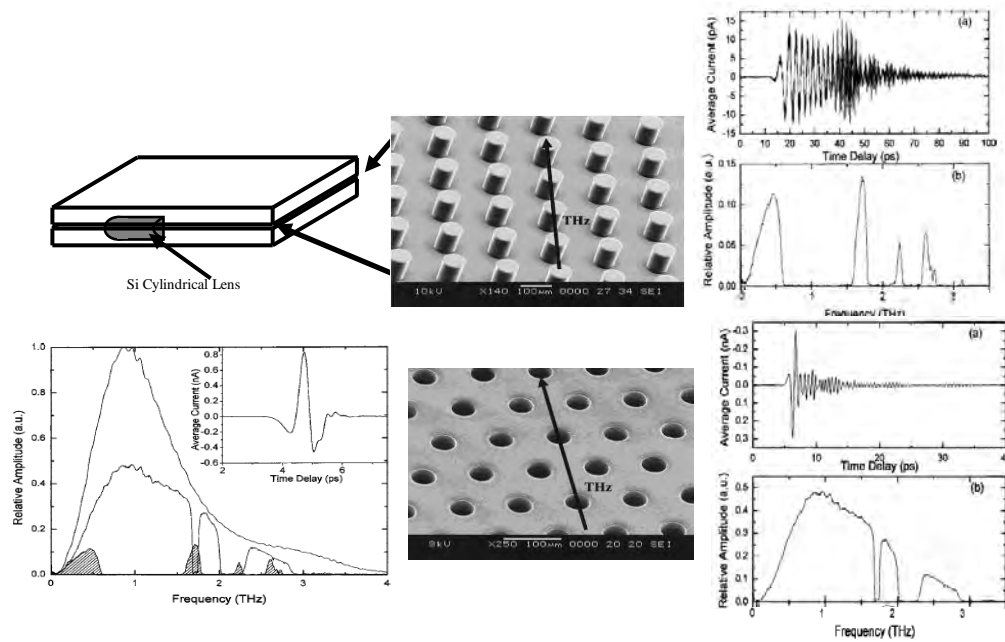


Fig. 9 2D Photonic Waveguides. The upper SEM image is the type I PBG surface. The lower SEM image is the type II PBG surface. The lower left diagram shows the normalized amplitude spectra from the reference (upper curve) and the sample pulses. The middle spectrum is from the type II photonic waveguide and the shaded spectrum is from the type I photonic waveguide. The inset shows the reference pulse. The upper set of diagrams (top right) show (a) Output THz pulse from type I photonic waveguide. (b) Amplitude spectrum of output pulse normalized to the reference pulse. The set of diagrams (lower right) show (a) Output THz pulse from type II photonic waveguide (b) Amplitude spectrum of output pulse normalized to reference pulse.

Due to the lack of spatial dependence of the TEM mode in the direction perpendicular to the plates of the PPWG, 3D PBG cylinder structures can be replicated in the 2D geometry of the PPWG. The initial conceptual plan for this experiment was to incorporate such 2D-PBG cylinder structures into the metal PPWG to control the frequency dependent transmission. This goal was to be achieved with high-precision 2D-PBG cylinder structures, fabricated by our new cleanroom based lithographic technique. Initially, we used a 2D-PBG structure of metal cylinders to fill the space between the two metal plates of the waveguide. However, the transmission through this structure was negligible. In order to increase the transmission, we broke the 2D-PBG symmetry by opening the space between the waveguide plates to let the tops of the 70- μm -tall metal cylinder (pillars) form one surface of the resulting 100 μm air gap to the second plate. For this theoretically more complex asymmetric system, we observed strong PBG transmission effects [19-20]. Our presented results describe this new class of air-spaced PPWGs, where a metallic PBG surface replaces one of the plates of the PPWG. The two complementary PBG

surfaces I and II shown in Fig. 9 allow controllable frequency filtering based on the dimensions, array design, and periodicity of the sample. The resulting THz photonic waveguides give high contrast frequency filtering, with the added benefits of air propagation and standard lithographic fabrication.

Closely related early microwave work on artificial dielectrics will now be presented.

The Artificial Dielectrics of Microwaves

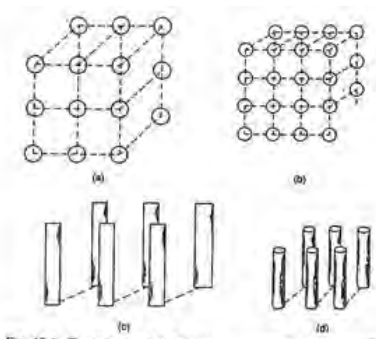
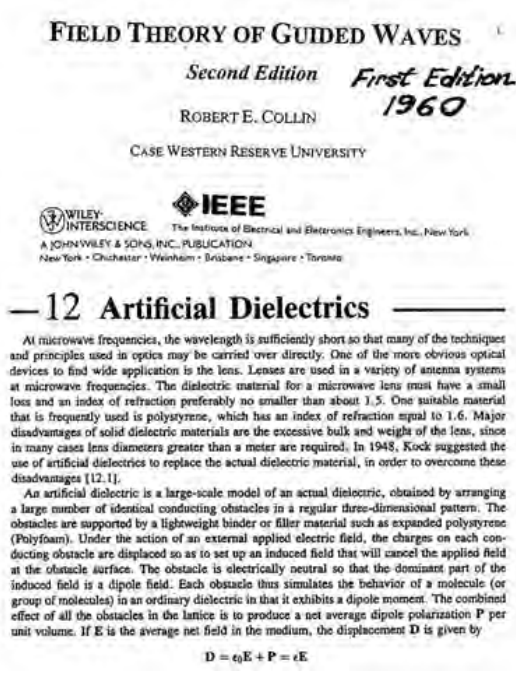


Fig. 12.1. Typical artificial dielectric structures (a) Three-dimensional sphere medium. (b) Three-dimensional disk medium. (c) Two-dimensional strip medium. (d) Two-dimensional rod medium.

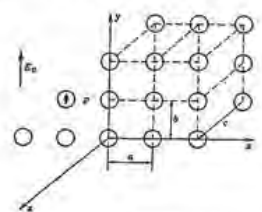


Fig. 12.2. A three-dimensional artificial dielectric medium.

Fig. 10 shows the artificial dielectric crystals of microwaves as presented in the classic textbook, “Field Theory of Guided Waves”, by Robert E. Collin and was published in 1960.

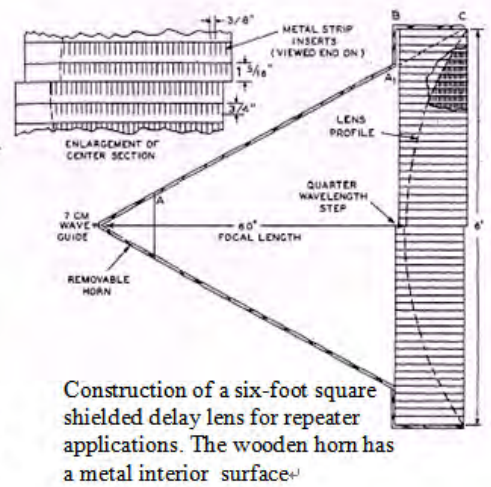
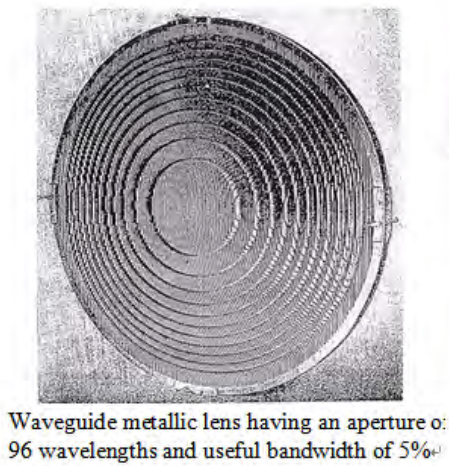


Fig. 11 Artificial dielectric lens with a 180 cm diameter and a 150 cm focus.

As shown in the above Fig. 10, the early microwave work on artificial dielectrics strongly overlaps the conceptual base of the photonic crystals of the optical and THz community. This early microwave work was driven by the desire to develop light-weight materials to use in the fabrication of the large quasi-optical components for microwave frequencies. An example of such a quasi-optical element is the waveguide coupling lens shown in the above Fig. 11, which is constructed of metal strips in a shifted lattice arrangement [21]. The lens has an aperture of 180 cm and a 150 cm focus onto a 7 cm waveguide.

4. THz Time domain spectroscopy (THz-TDS)

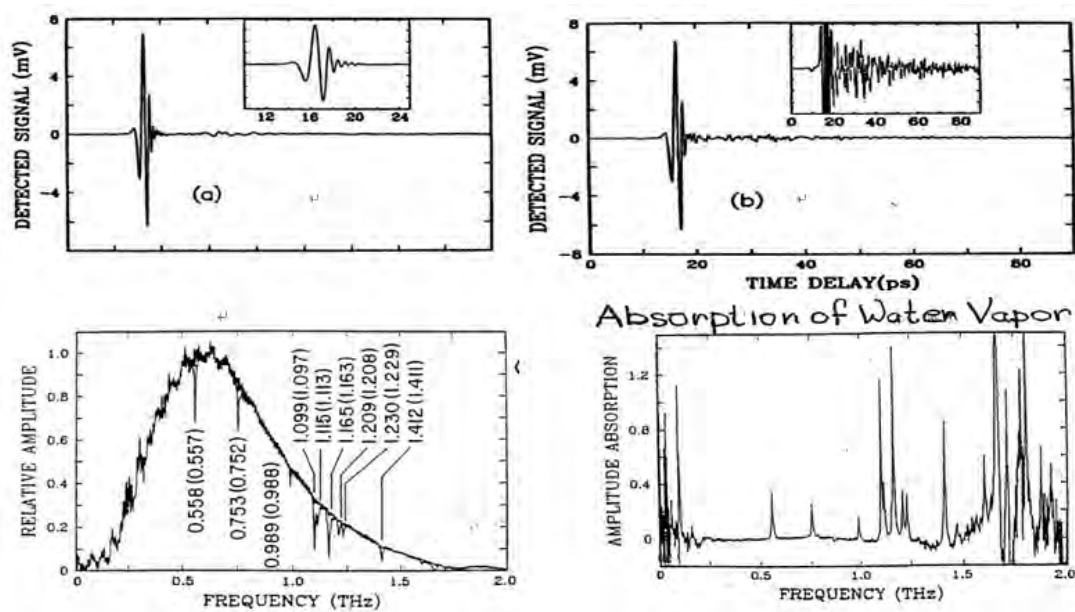


Fig.12 The first THz-TDS measurement of water vapor.

For this measurement [6] the air-tight enclosure of the THz-TDS system shown in Fig. 4 was filled with nitrogen vapor to make the reference measurement of the transmitted THz pulse (nitrogen pulse). Then 1.5 Torr of water vapor (8% humidity at $20.5\text{ }^{\circ}\text{C}$) was added to the enclosure and the transmitted water vapor pulse was measured. The numerical amplitude spectrum for the water pulse was divided by the amplitude spectrum of the nitrogen pulse to obtain the frequency dependent amplitude transmission. The natural logarithm of the transmission gave the absorbance. THz-TDS has since been used for more than one thousand measurements worldwide. THz-TDS has significantly better S/N than far-infrared FTS for frequencies below 5 THz . We will now describe the recent and most accurate (to date) THz-TDS measurements of the atmosphere.

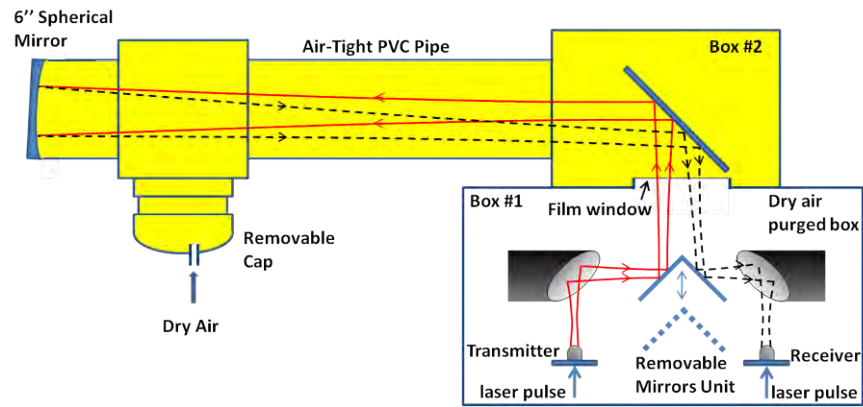


Fig. 13 THz-TDS set-up and results for the controlled measurement of the absorption of water vapor for a 6.18 *m* round-trip path.

The measurement uses the standard THz-TDS system shown in Fig. 4 with removable coupling mirrors [22]. The coupling into and out of the sample tube is excellent. The air-tight end of the sample tube holds a six-inch (15 *cm*) diameter gold-coated spherical mirror with a radius of curvature of 120 *inches* (305 *cm*), and the center of curvature is located at the THz beam waist of the THz-TDS system. The humidity of the sample tube (highlighted in yellow) was reduced to less than 0.5% at 21 °C for the reference dry-air transmitted pulse shown in the figure, and could be easily increased to the humidity level of the laboratory (RH 51% at 21 °C).

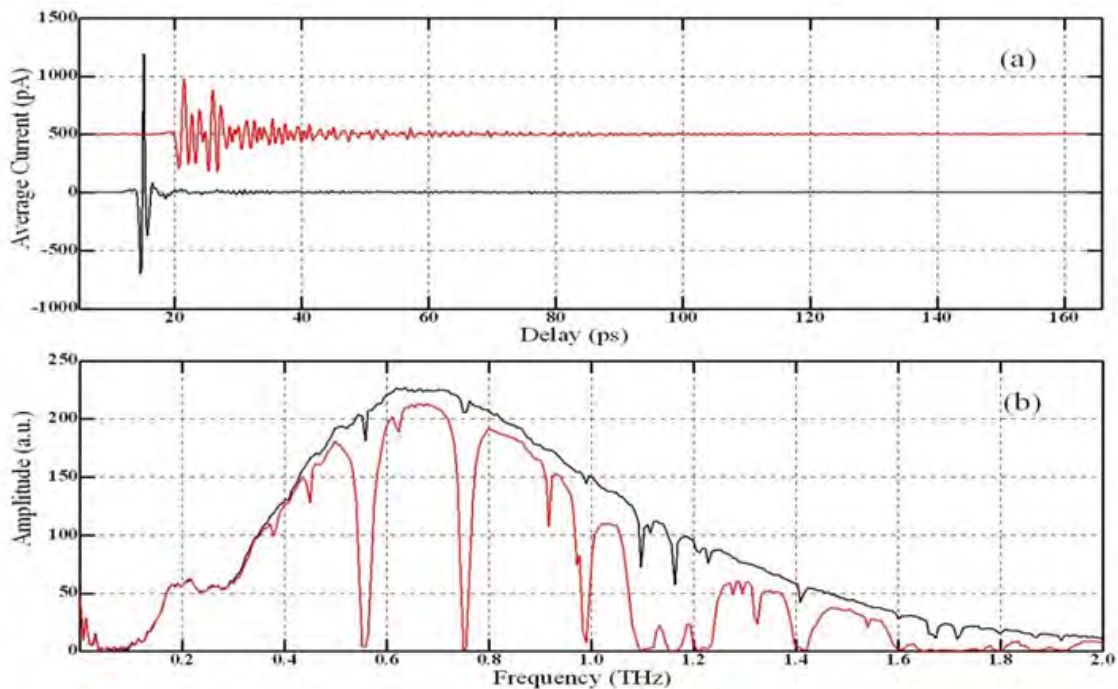


Fig. 14 (a) Measured THz reference pulse (lower trace) and measured THz sample pulse (upper trace). For clarity the THz sample pulse was shifted upwards by 500 *pA*. (b) Corresponding amplitude spectrum (upper curve) for the THz reference pulse and the amplitude spectrum (lower curve) for the sample pulse.

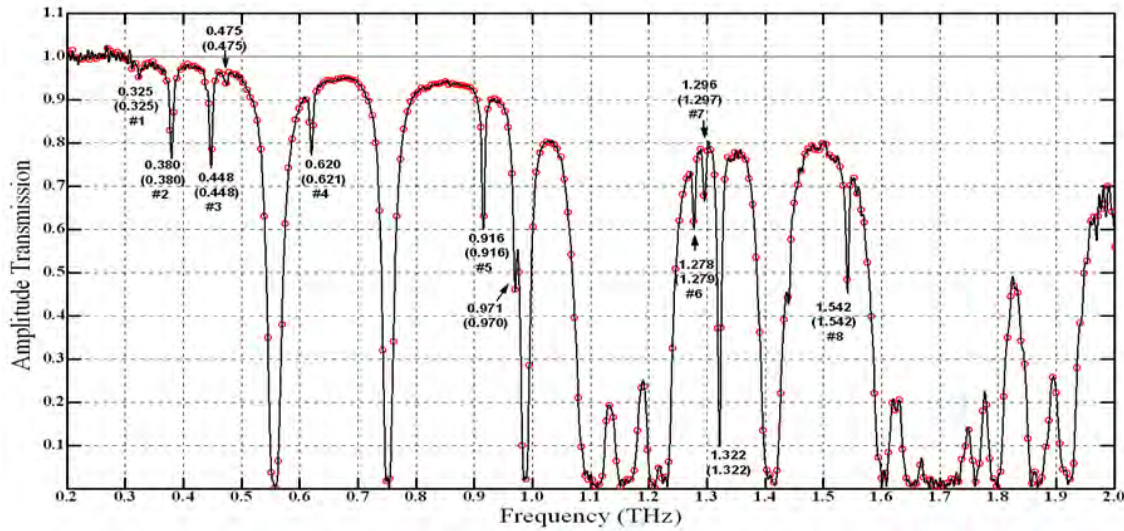


Fig. 15 Amplitude transmission through 6.18 m of the atmosphere at 21 °C and with RH 51%. The amplitude transmission was obtained from the ratio of the amplitude spectrum of the sample pulse to the amplitude spectrum of the reference pulse as shown in Fig. 14.

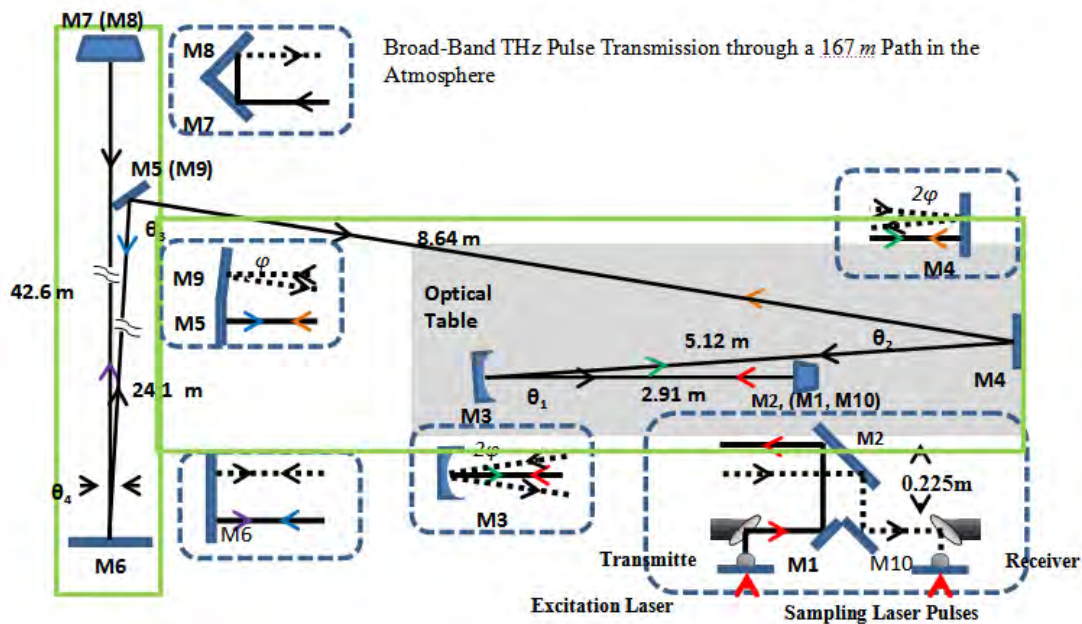


Fig. 16 THz long-path set-up.

The amplitude transmission shown in the above Fig. 15 is simply the ratio of the sample spectrum to the reference spectrum of Fig. 14b. For this result, the “real data points” are indicated by the larger open circles separated from each other by 6.1 GHz, and the interpolated points obtained from the zero-padding are separated from each other by 0.61 GHz and define the solid line. The weaker water lines appear with their expected frequencies, strengths and with linewidths equal to the spectral resolution of 6.1 GHz. The central frequency of the measured water lines is determined to an accuracy of ± 1 GHz as indicated in Fig. 15. The frequency in

parenthesis is the accepted handbook value. Only water lines are observed. This high resolution measurement provides the most accurate THz-TDS results to date for the transmission windows and the absorption strengths of the weak lines of the water vapor transmission of the atmosphere. These results together with the THz pulse long-path measurements to be described in the next section show possibilities for atmospheric sensing, imaging and ranging for more than 100 *m*.

The round trip path shown in the above Fig 16 is 166.84 *m*, precisely equal to 50 round-trip paths of the ultrafast mode-locked Ti-Sapphire laser with the pulse repetition rate of 89.82 *MHz* [23]. Consequently, for a given laser excitation pulse to the THz transmitter, the corresponding sampling pulse is 50 *pulses* later down the pulse train. The standard THz-TDS system with removable coupling mirrors is the transceiver. The system stability is surprisingly good, considering that mirrors M5-M9 are supported by the floors of the laboratory and our long connecting hallway. The remaining set-up is on the floating optical table. The THz transceiver is driven by two 10 *mW* average power ultrafast laser beams, and 30 *nW* of average THz power is incident on the coupling mirror M3.

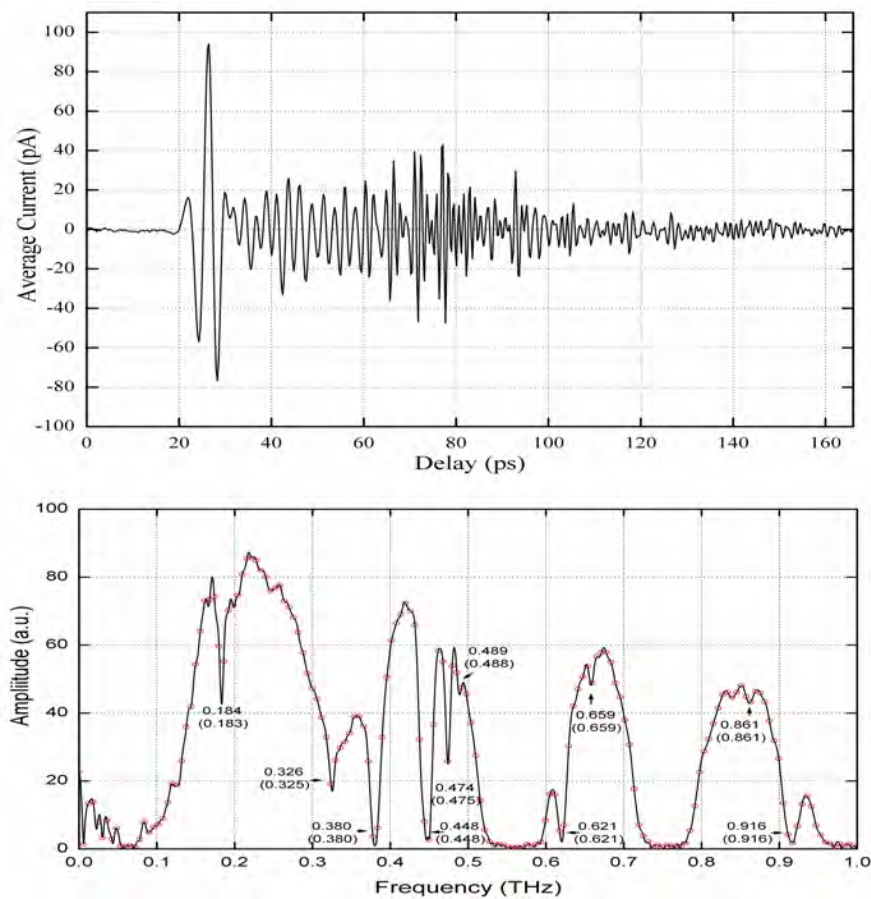


Fig. 17 Long-path transmitted THz pulse and corresponding amplitude spectrum.

Under typical conditions of RH 51% at 21°C as shown in Fig. 17, the return beam after traversing the 167 *m* path has an average power of 130 *pW*. The ability to measure such low powers with the excellent S/N is due to the coherent gating of the receiver by the 80 *fs* ultrafast

sampling pulses. The measured transmitted pulse has been attenuated and broadened by passage through the water vapor. The corresponding amplitude spectrum of this pulse displays the weak water lines to 1 GHz accuracy compared to the handbook values shown in parentheses. These results clearly show potential for stand-off sensing.

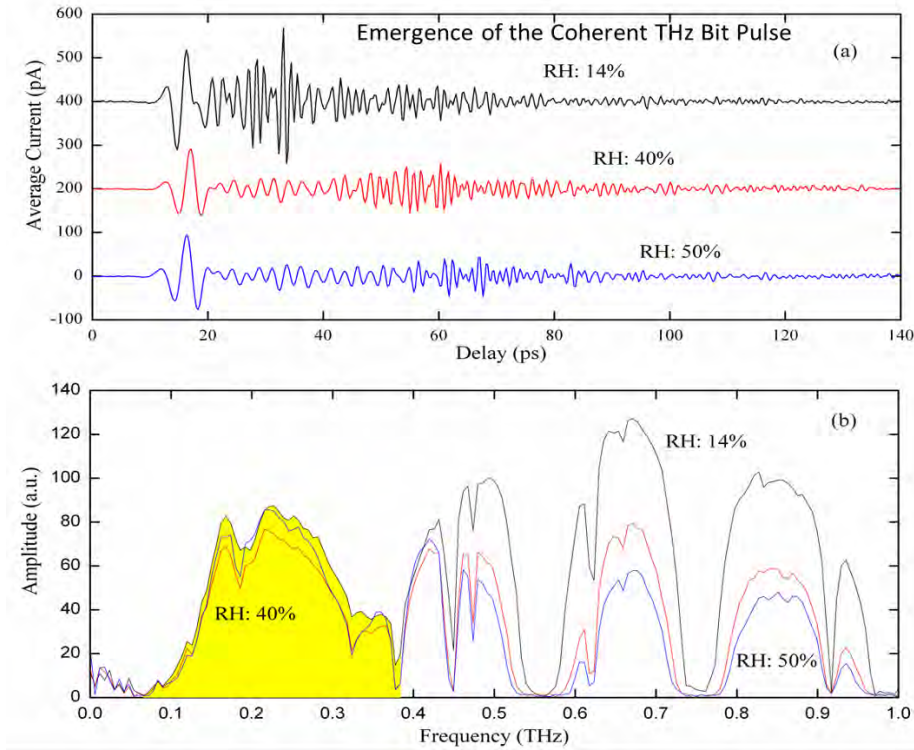


Fig. 18 Emergence of the coherent THz bit pulse on the leading edge of the transmitted long-path pulse through a humid atmosphere

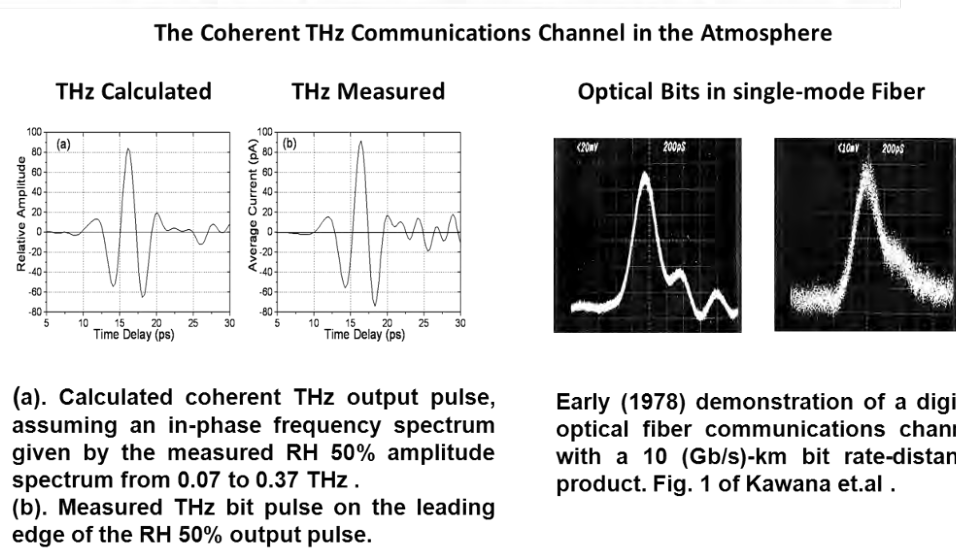


Fig. 19 The observed THz bit pulse is compared a calculated fully coherent pulse. These pulses are then compared to optical bit pulses.

This THz bit pulse can be understood as the coherent propagation of the frequency components from 0.07 to 0.37 THz of the input impulse THz pulse for which all the frequency components from 0.07 to 1.8 THz are in phase. During propagation through the humid path, all the frequency components above 1 THz are absorbed, while the frequency components from 0.07 to 1.0 THz are selectively absorbed by the strong water lines, and the entire propagating pulse is also broadened by the group velocity dispersion (GVD). However, the frequency components from 0.07 to 0.37 THz (highlighted in yellow) are not absorbed and propagate with no GVD. Consequently, these components emerge as a transform limited pulse at the end of the path. As shown in Fig. 19, this concept was confirmed by performing the inverse numerical Fourier transform for the measured amplitude spectrum from 0.07 to 0.37 THz assuming phase coherence. As shown, the calculated pulse is in excellent agreement with the measured pulse.

The importance of this result to THz communications is illustrated by the following example. Using the THz bit pulse with a bit rate of 50 GHz and the path length of 0.167 km, the Bit rate distance product is 8.4 (Gb/s)-km, comparable to a second-generation, single-mode optical fiber communications channel [24], as also shown in Fig.19.

5. Conclusions

It is important to connect the recent THz work to the extensive microwave literature, because all of the THz guided wave demonstrations to date have their microwave counterparts, and because for both THz and microwaves, the real part of metal conductivity can be considered to be frequency independent and equal to the handbook value. Compared to microwaves, THz phenomena occur at a smaller spatial scale proportional to the shorter wavelengths. The corresponding frequency dependent losses are higher and the skin depths are smaller, but the basic phenomena are the same. The smaller THz spatial scale is especially convenient for the use of quasi-optics, and also enables easy lithographic fabrication of photonic surfaces and two dimensional photonic lattices. The concept of digital THz communications is enabled by the broad bandwidths available in the THz band.

References

- [1] D.H. Auston, "Ultrafast Optoelectronics", "Ultrashort Laser Pulses and Applications", 1st. Edn., ed. by W. Kaiser, *Topics Appl. Phys.* (Springer, Berlin, Heidelberg), 183-233. (1988)
- [2] M.B. Ketchen, D. Grischkowsky, T.C. Chen, C-C. Chi, I.N. Duling,III, N.J. Halas, J-M Halbout, J.A. Kash, and G.P. Li, "Generation of Sub-Picosecond Electrical Pulses on Coplanar Transmission Lines", *Appl. Phys. Lett.* 48, 751-753, (1986).
- [3] D. Grischkowsky, "Optoelectronic Characterization of Transmission Lines and Waveguides by THz -TDS", *IEEE Journal of Selected Topics in Quantum Electronics*, 6, 1122-1135, (2000).
- [4] D. Grischkowsky, I.N. Duling III, J.C. Chen and C-C. Chi, "Electromagnetic Shock Waves from Transmission Lines", *Phys. Rev. Lett.* 59, 1663-1666, (1987).

- [5] Ch. Fattinger and D. Grischkowsky, "Point Source TeraHz Optics", *Appl. Phys. Lett.* 53, 1480-1482, (1988).
- [6] M. van Exter, Ch. Fattinger and D. Grischkowsky, "TeraHz Time Domain Spectroscopy of Water Vapor", *Optics Letters*, 14, 1128, (1989).
- [7] M. van Exter and D. Grischkowsky, "Characterization of an Optoelectronic TeraHz Beam System", *IEEE Transactions on Microwave Theory and Techniques*, 38, 1684-1692, (1990).
- [8] D. Grischkowsky, S. Keiding, M. van Exter and Ch. Fattinger, "Far-Infrared Time-Domain Spectroscopy with TeraHz Beams of Dielectrics and Semiconductors", *J. Opt. Soc. B.* 7, 2006-2015, (1990).
- [9] Jianming Dai, Jiangquan Zhang, Weili Zhang and D. Grischkowsky, "THz Time-Domain Spectroscopy (THz-TDS) Characterization of the Far-Infrared Absorption and Index of Refraction of High-Resistivity, Float-Zone Silicon", *J. Opt. Soc. Am. B.* 21, 1379-1386, (2004).
- [10] C. Johnson, F. J. Low, and A. W. Davidson, "Germanium and germanium-diamond bolometers operated at 4.2 K, 2.0 K, 1.2 K, 0.3 K, and 0.1 K", *Opt. Engr.*, 19, 255, (1980)
- [11] A. A. Penzias and R. W. Wilson, "Measurement of the Flux Density of CAS A at 4080 Mc/s", *Astrophysical Journal*, 142, 1149-1155, (1965).
- [12] G. Gallot, S. Jamison, R.W. McGowan and D. Grischkowsky, "THz Waveguides", *J. Opt. Soc. Am. B.* 17, 851-863, (2000).
- [13] R. Mendis and D. Grischkowsky, "Undistorted guided wave propagation of subpssec THz pulses", *Optics Letters*, 26, 846-848, (2001).
- [14] Jiangquan Zhang and D. Grischkowsky, "Waveguide THz time-domain spectroscopy of nm water layers", *Optics Letters*, 29, 1617-1619, (2004).
- [15] J. S. Melinger, N. Laman, S. Sree Harsha, and D. Grischkowsky, "Line Narrowing of THz Vibrational Modes for Organic Thin Films within a Parallel Plate Waveguide", *Appl. Phys. Lett.* 89, 251110, (2006).
- [16] R. Mendis and D. Grischkowsky, "THz Interconnect with Low Loss and Low Group Velocity Dispersion", *IEEE Microwave and Wireless Components Lett.* 11, 444-446, (2001).
- [17] Michael Theuer, S. Sree Harsha, and D. Grischkowsky, "Flare Coupled Metal Parallel-Plate Waveguides for High Resolution THz-TDS", *J. Appl. Phys.* 108, 113105, (2010).
- [18] Jiangquan Zhang and D. Grischkowsky, "Adiabatic compression of parallel-plate metal waveguides for sensitivity enhancement of waveguide THz time-domain spectroscopy", *Appl. Phys. Lett.* 86, 061109, (2005).
- [19] Adam Bingham, Yuguang Zhao, and D. Grischkowsky, "THz Parallel Plate Photonic Waveguides", *Appl. Phys. Lett.*, 87, 051101, (2005).
- [20] Y. Zhao and D. Grischkowsky, "Terahertz demonstrations of effectively 2D photonic bandgap structures", *Optics Letters*, 31, 1534-1536, (2006).
- [21] W. E. Kock, "Metallic delay lenses," *Bell Syst. Tech. J.*, 27, 58-82, 1948

- [22] Yihong Yang, Alisha Shutler, and D. Grischkowsky, "Measurement of the transmission of the atmosphere from 0.2 to 2 THz", *Optics Exp.* 19, 8830-8838, (2011).
- [23] Yihong Yang, Mahboubeh Mandehgar and D. Grischkowsky, "Broad-Band THz Pulse Transmission through the Atmosphere", *IEEE Trans. on THz Science and Technology*, 1, 264-273, (2011).
- [24] A. Kawana et.al. "Pulse broadening in long-span, single-mode optical fibers around a material-dispersion-free wavelength", *Opt. Lett.* 2 106-108, (1978).